JGR Oceans

RESEARCH ARTICLE
10.1029/2023JC019837

Observed and Projected Changes in North Atlantic Seasonal Temperature Reduction and Their Drivers

Jeremy P. Grist[1], **Simon A. Josey**[1], **and Bablu Sinha**[1]

[1]National Oceanography Centre, Southampton, UK

Key Points:

- Analysis reveals that the Autumn seasonal decline in North Atlantic sea surface temperature (SST) has strengthened in recent decades
- The changes in the Sub Polar Gyre are associated with a greater sensitivity of SST to surface heat loss due to increased stratification
- Changes in regions influenced by sea-ice are associated with greater surface heat loss

Correspondence to:
J. P. Grist,
jeremy.grist@noc.ac.uk

Citation:
Grist, J. P., Josey, S. A., & Sinha, B. (2023). Observed and projected changes in North Atlantic seasonal temperature reduction and their drivers. *Journal of Geophysical Research: Oceans*, *128*, e2023JC019837. https://doi.org/10.1029/2023JC019837

Received 20 MAR 2023
Accepted 27 OCT 2023

Abstract The autumn-winter seasonal temperature reduction (STR) of the surface North Atlantic Ocean is investigated with control and climate change simulations of a coupled model and an observation-based sea surface temperature (SST) data set. In the climate change simulation, an increase in the magnitude of the STR is found over much of the North Atlantic, and this change is particularly marked in sea-ice affected regions and the subpolar gyre. Similar results for the mid-high latitude North Atlantic are obtained in the observational analysis. In particular, both the observation and climate model based results show that the STR has increased in magnitude by up to 0.3°C per decade in the subpolar gyre over the period 1951–2020. Drivers for the stronger STR are explored with a focus on potential contributions from increases in either ocean heat loss or the sensitivity of SST to heat loss. Over a large part of the mid-high latitude North Atlantic surface heat loss is found to have weakened in recent decades and is therefore not responsible for the stronger STR (exceptions to this are the near-coastal areas where sea-ice loss is important). In contrast, analysis of daily sensible and latent heat flux data reveals that the sensitivity of SST to heat loss has increased indicating that this term has played a major role in the stronger STR. Areas of greater SST sensitivity (and greater STR) are associated with increased surface stratification brought about predominantly by warming of the northern ocean regions.

Plain Language Summary Every autumn there is a seasonal drop in the sea surface temperature (SST) of the North Atlantic Ocean. We show that in recent years the size of this drop has been increasing and it is projected to decline further in coming decades. Both historical observations and a climate model simulation show that this seasonal temperature reduction has increased in magnitude by up to 0.3°C per decade in the subpolar gyre over the period 1951–2020. We show that the cause of the increase in temperature drops depends on the specific area of the North Atlantic. In the Subpolar Gyre surface heat loss is found to have weakened in recent decades and is therefore not responsible for the larger SST decline. The decline in that area is instead associated with the ocean surface temperature becoming more sensitive to heat flux, due to the increase in the surface stratification. However, in those regions partially covered by sea-ice, a decline in sea-ice coverage, and a corresponding increase in surface heat loss is the cause of the larger autumn SST decline. Finally, the changes in autumn cooling result in stronger north-south gradient in SST which may enhance the storminess of mid-latitude winter weather systems.

1. Introduction

The projected response of Sea Surface Temperature (SST) to global warming shows marked spatially variability in the North Atlantic. For example, a region of reduced warming in the subpolar gyre, known as the "warming hole" is often attributed to a decline in the Atlantic Meridional Overturning Circulation (AMOC) (Drijfhout et al., 2012). In addition, enhanced warming on the North-West Atlantic shelf has been attributed to movement in the location of the Gulf Stream (Grist et al., 2021; Saba et al., 2016).

In these examples, spatial variability is explained by changes in the ocean circulation. However, in regions which exhibit a strong seasonal dependence of SST changes, additional processes including air-sea, and ice-sea interaction need to be considered. Studies with CMIP5 models have indicated that SST warming trends are greater in summer than in winter (Alexander et al., 2018; Chen & Wang, 2015). This difference has been primarily attributed to the shallower (and decreasing) summer mixed layer resulting in a smaller water volume being acted on by surface heat fluxes (Gallego et al., 2018). However, the geographical variability of both the changes and the mechanisms responsible for the changes have not been fully ascertained (Liu et al., 2020; Timmermann et al., 2004). Indeed, earlier studies with CMIP3 models, found a reduction in the seasonal SST in region such as the Nordic Seas, Labrador Sea, and parts of the Tropical Atlantic Ocean (Dwyer et al., 2012; Sobel & Camargo, 2011).

In this study, we examine long-term changes in North Atlantic autumn cooling using observations and climate change simulations obtained with a coupled model. Our goal is to examine the spatial variability of candidate drivers of the long-term changes, with attention given to specific processes potentially related to Arctic climate change. The implications of the long-term changes in autumn cooling for regional weather and climate are also discussed.

The structure of the paper is as follows. In Section 2, the observations and model simulations used are described as well as details of the analysis undertaken. In Section 3, the results are presented in three parts. First, the long-term changes in seasonal temperature reduction (STR) of the North Atlantic are examined. Second, candidate causes of the changes in STR are investigated. Third, the implications of the changes in STR for regional weather and climate are discussed. Finally, in Section 4 our results are summarized.

2. Model, Simulations, Analysis

The model used is the Hadley Center Global Environment Model 3—Global Coupled vn 3.1 (HadGEM3-GC3.1-HM) (Williams et al., 2017). It has a 25 km atm and an eddy-permitting (~25 km, ¼°) ocean, with 75 levels in the vertical (Roberts et al., 2019). We establish the climate change signal by examining the 1950–2050 climate change projection of the model. The projection has two parts, 1950–2014 is the historical forcing simulation (hist-1950, Roberts, 2018a) and 2015–2050 is a future projection (highres-future, Roberts, 2019). Time-varying external forcings follow the SSP585 future scenario (Riahi et al., 2017). Designed to represent emissions high enough to produce a radiative forcing of 8.5 W m $^{-2}$ in 2100, SSP585 is the most similar CMIP6 scenario to RCP8.5 in CMIP5. The spin-up protocols are described in Roberts et al. (2019). To establish the climate change signal, we examine century-long time series and trends in the relevant 1950–2050 climate change projections. The 95% significance of the trends are calculated, assuming the effective number of degrees of freedom, taking account the auto-correlation of the time series (Santer et al., 2000). In addition, the relationship between stratification and autumn cooling is investigated using the control run ("control-1950") (Roberts, 2018b). The control run is a 100-year simulation with constant radiative forcing using the 10-year 1950s climatology (Haarsma et al., 2016). The model simulations are compared to 40 years of ERA5 reanalysis (1981–1982 to 2020–2021, Hersbach et al., 2020).

The analysis considers the STR, defined as February SST minus SST of the previous October. Calculations of this term in the model are compared with corresponding fields of the HadISST SST data set (Rayner et al., 2003). The summer surface stratification, here defined as the potential density at the 100 m depth level minus the same at the surface level for June, July, and August (JJA) is also calculated. We also calculate SST sensitivity, specifically the sensitivity of SST to a unit change of surface turbulent heat flux. Turbulent heat flux is the sum of the latent and sensible heat flux components, the dominant sources of heat flux variability in the region of interest. The SST sensitivity (°C/Wm^{-2}) is the slope of a linear regression of daily SST values against the daily turbulent heat flux values. Although non-linear fits may explain more variance in certain regions with extreme fluxes, the linear fit is robust and easily interpreted. The slope is calculated for each individual autumn-winter period using the days spanned by the STR definition, that is, October, November, December, January, and February (ONDJF) for each (model or observational) grid point. We note that over the domain considered October (February) is typically one of the warmest (coldest) 3 months of the year and so changes in the STR are indicative of changes in the seasonal cycle as a whole. The sign convention adopted for the turbulent heat flux is for negative values to represent ocean heat loss to the atmosphere. We note that the SST sensitivity employed here is the inverse of a measure termed the heat flux feedback previously employed in studies of the heat flux - SST relationship at longer month to month timescales (Frankignoul & Kestenare, 2002; Frankignoul et al., 1988, 2004). Frankignoul et al. (1988) show that the cross correlation between surface heat flux and SST anomalies changes sign between negative and positive lag, indicating the heat flux damps an SST anomaly over several months once it has contributed to its initial development (i.e., the heat flux exhibits a negative feedback). The relationship between the diagnostics calculated here with those in Frankignoul et al. (1988) across the transition from daily to monthly timescales is an interesting topic which we propose to examine in future work.

3. Results

3.1. Long-Term Changes in Seasonal SST Decrease

The climatological mean reduction of SST between October and the following February (which we term STR) in the HM climate change simulation is shown in Figure 1a. The magnitude of STR ranges up to 10°C along the

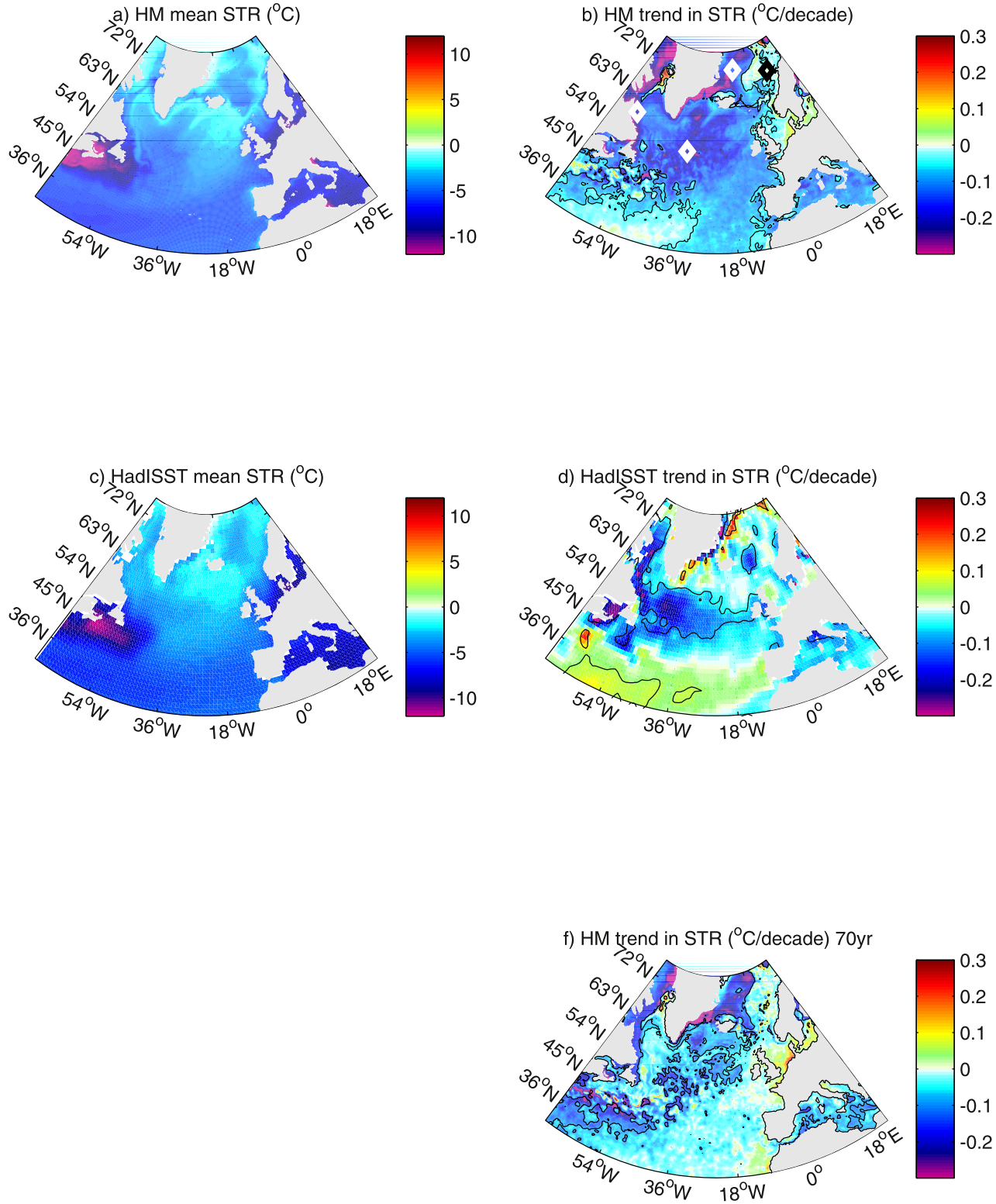

Figure 1. Mean seasonal temperature reduction (STR between February sea surface temperature (SST) and SST from previous October (°C)) in panel (a) HM climate projection simulation 1950–2050 and (c) HadISST observations 1951–2020. Trend (°C/decade) in STR for (b) HM 1951–2050; (d) HadISST 1951–2020 and (e) HM 1951–2020. White and black diamonds in panel (b) denote locations of time series in Figure 2. Black contours denote 95% significance level.

US coast with more typical values of 2°C–5°C in the subpolar gyre and higher latitudes which are our primary regions of interest. The trend of STR over the period 1951–2050 is shown in Figure 1b, it is evident that for much of the North Atlantic the magnitude of the temperature decline between October and February increases that is, the seasonal cooling has become stronger over the past 70 years. The pattern of the STR trend (Figure 1b) is broadly speaking a reversal of the mean field (Figure 1a) with a greater seasonal cooling trend in the subpolar gyre (−0.15 ± standard error 0.02 to −0.30°C ± 0.06°C per decade) than further south and values as strong as −0.45°C ± −0.08°C per decade along the Greenland coast.

The corresponding observed (HadISST) mean and trend in STR are shown in Figures 1c and 1d). The long-term mean is very similar to that in HM and the pattern of the STR trend shows agreement in the key mid-high latitude features. These include the broad negative trend (i.e., enhanced seasonal cooling) over the subpolar gyre between 45°N and 65°N and larger negative trends in regions of declining sea-ice, such as the western Labrador Sea and Western Baffin Bay. We note the HM trend over the historical period (Figure 1e) is broadly similar to the 1951–2050 trend. The most noticeable difference being that in the SPG the projected trend (Figure 1b) is greater than the observational period. The observed trend in the between 45°N and 65°N lies between that of the simulation over the historical period (Figure 1e) and the full period (Figure 1b). An area of difference between the observations and the model is between 20°N and 40°N where the model trend is weakly negative and the observed trend is positive. However, at mid-high latitudes, the similarities between HM and observations suggests the projected changes are reliable and motivate a greater understanding of both their drivers and any implications for the overlying atmospheric conditions.

To investigate the trends further, we plot time series for selected locations, denoted by four diamonds (three white and one black) in Figure 1b. In the Subpolar Gyre (35°W, 53°N), the trend in Autumn temperature drop arises as the October temperature increases and the February temperature decreases slightly (Figures 2a and 2b). In the Labrador Current (61°W, 58°N), an increase in STR occurs due to a steadily increasing October SST and a February SST that remains constant. The near constant value for February is indicative of the area remaining under sea-ice out to 2050, despite ocean warming elsewhere. The observations are broadly similar, but with a less consistent constraint of February sea-ice cover, there is some interdecadal variability in February SST (Figures 2c and 2d). In the West Greenland Sea (12°W, 72°N), there is a 5°C increase in October SST over the 100-year period, with accelerated growth after 2000 (Figure 2e). The February SST stays predominantly close to −2°C until 2020 when it increases to 0°C, it then exhibits some interannual variability, returns to −2°C in 2030, and then increases rapidly to approximately 2.5°C by 2050. So, relative to October, the February temperature increase starts later and occurs in steps. The net result is that while there is a long-term trend of STR increasing (i.e., becoming more negative), there is considerable variability around this trend (Figure 2f). Like the Labrador Current the extent of the difference in sea-ice coverage between October and February appears to be an important influence on the STR increase. Finally, in the Norwegian Sea (10°E, 70°N), the October and February SST show similar rates of increase (about 4°C over the 100 years) (Figure 2g), consistent with observations. As the October and February SSTs track each other there is no noticeable long-term change in autumn cooling. Aside from some interannual variability, STR remains at about −2°C between October and the following February (Figure 2h). Note that, despite its northern latitude, as the region is ice-free all year round, this is an area where one would expect minimal influence from Arctic sea-ice decline or freshwater input. Overall, these examples indicate there are a range of scenarios that can lead to increase (or lack thereof) in autumn cooling. This suggests that although the cooling trend is largely in one direction over the north Atlantic (Figure 1a), more than one process is likely to be responsible, depending on the specific region.

In general, an increasing magnitude of the STR could be due either to (a) an increase in the sensitivity of the ocean SST to surface heat flux or (b) an increase in ocean surface heat loss with fixed SST sensitivity. We first consider the sensitivity of the ocean to the turbulent air-sea fluxes and then consider the trends in the air-sea fluxes. With regard to the sensitivity, for each year we use ONDJF daily turbulent heat flux and ONDJF daily SST to calculate the turbulent heat flux-SST slope in °C per W m^{-2}. An example of such a slope is shown in Figure 3a. We then calculate the mean ONDJF slope from the 100 years of the HM simulation and 40 years of ERA5 reanalysis (Figures 3b and 3c, respectively). With this diagnostic, the more positive the slope is the more easily the SST is changed by a given amount of turbulent heat flux change. Much of the extra-tropical North Atlantic has a positive slope. The greatest positive slopes are in the northern latitudes, particularly in the western subpolar gyre as well as the Norwegian and Barents Sea. This indicates that these are regions where the SST is more easily changed by

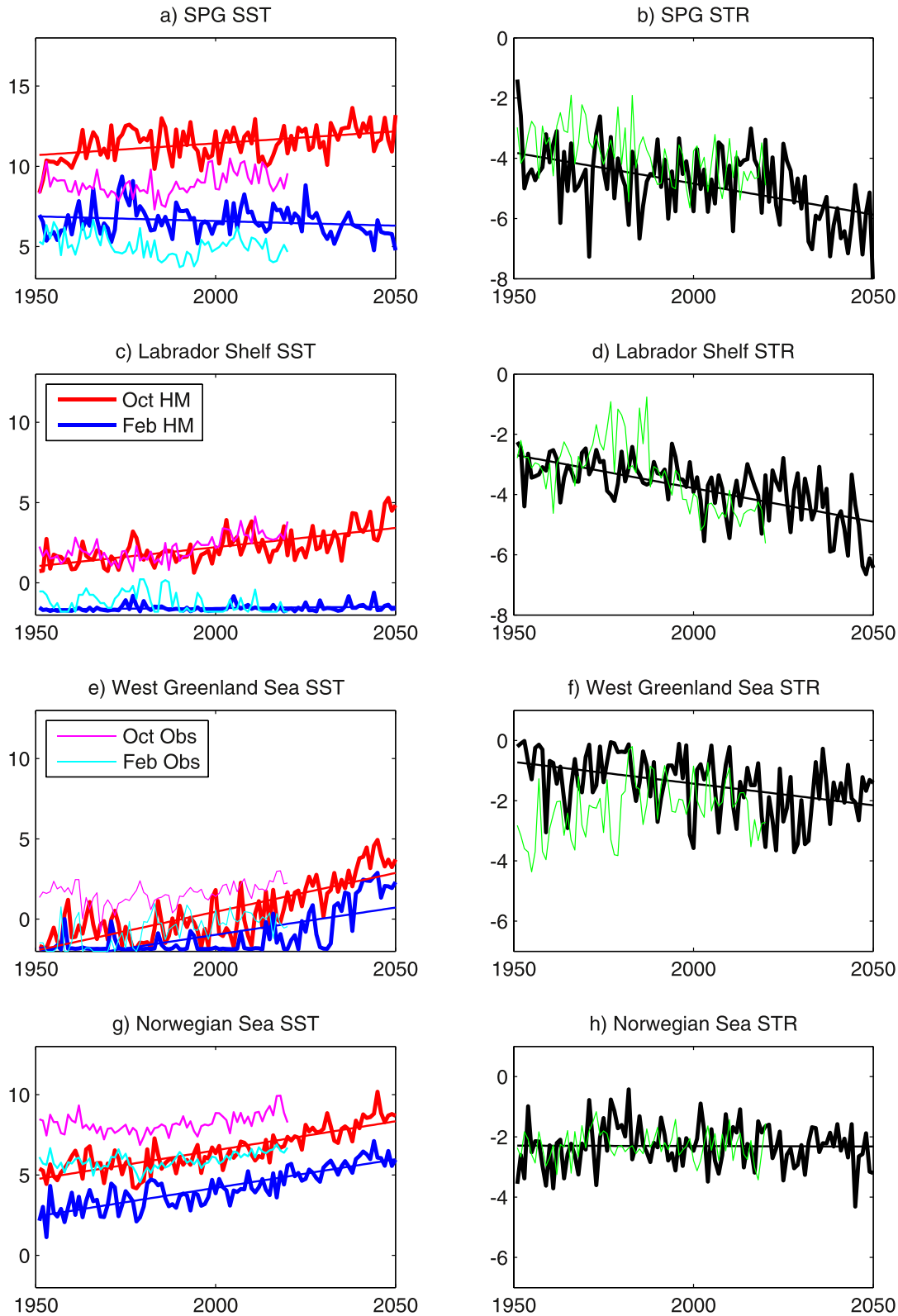

Figure 2. October (red-model and magenta-observations) and following February (blue-model and cyan-observations) sea surface temperature (SST) time series for grid points in selected regions (shown in Figure 1b) of North Atlantic: (a) SPG, (c) Labrador Sea, (e) West Greenland Sea and (g) Norwegian Sea. Panels (b), (d), (f), and (h) are the corresponding figures of the February minus October SST difference (STR) (black-model and green-observations). The linear trend for the model is also displayed in all panels. Statistical details of linear trends are shown in Table 1.

Table 1
Statistical Details of Linear Trends Calculated in Figure 2.

Panel and color	Area	Month	Model/obs.	Trend deg/decade ± s.e	Signif. at 95% level
(a) Red	SPG	October	Model	0.15 ± 0.03	Y
(a) Blue	SPG	February	Model	−0.06 ± 0.03	N
(b) Black	SPG	February minus October	Model	−0.21 ± 0.04	Y
(a) Magenta	SPG	October	Obs.	0.11 ± 0.04	Y
(a) Cyan	SPG	February	Obs.	−0.12 ± 0.04	Y
(b) Green	SPG	February minus October	Obs.	−0.22 ± 0.04	Y
(c) Red	Labrador	October	Model	0.24 ± 0.03	Y
(c) Blue	Labrador	February	Model	0.02 ± 0.03	Y
(d) Black	Labrador	February minus October	Model	−0.22 ± 0.03	Y
(c) Magenta	Labrador	October	Obs.	0.24 ± 0.03	Y
(c) Cyan	Labrador	February	Obs.	−0.11 ± 0.00	Y
(d) Green	Labrador	February minus October	Obs.	−0.35 ± 0.05	Y
(e) Red	WGS	October	Model	0.48 ± 0.04	Y
(e) Blue	WGS	February	Model	0.34 ± 0.04	Y
(f) Black	WGS	February minus October	Model	−0.14 ± 0.03	Y
(e) Magenta	WGS	October	Obs.	0.12 ± 0.04	Y
(e) Cyan	WGS	February	Obs.	0.28 ± 0.04	Y
(f) Green	WGS	February minus October	Obs.	0.16 ± 0.05	Y
(g) Red	Nor Sea	October	Model	0.361 ± 0.02	Y
(g) Blue	Nor Sea	February	Model	0.36 ± 0.02	Y
(h) Black	Nor Sea	February minus October	Model	0.00 ± 0.03	N
(g) Magenta	Nor Sea	October	Obs.	0.13 ± 0.03	Y
(g) Cyan	Nor Sea	February	Obs.	0.12 ± 0.02	Y
(h) Green	Nor Sea	Feb minus October	Obs.	−0.01 ± −0.03	N

Note. SPG is subpolar gyre (panels a and b), Labrador is Labrador Shelf (panels c and d), WGS is West Greenland Sea (panels e and f); nor Sea is Norwegian Sea (panels g and h).

air-sea heat exchange. Regions of negative slope, such as the Gulf Stream Extension region and the south-eastern North Atlantic, express the extent that SST change will cause changes in turbulent heat flux.

We now examine potential trends in the heat flux–SST relationship that is, whether the SST is becoming more or less sensitive to the turbulent heat loss. For this analysis, we fit a linear trend to the set of individual winter sensitivity estimates at each grid point, see Figure 4. In the HM climate change simulation, it is evident that north of 54°N the trend is positive. This indicates in this region SST becomes more sensitive to the turbulent heat flux, that is, consistent with the increasing magnitude of STR, the SST is becoming more easily altered by the air-sea flux. This is evident in the subpolar Gyre but is also particularly enhanced in the Greenland-Nordic Sea region. In the ERA5 reanalysis (Figure 4b), the regions of increasing sensitivity are more limited, but the region immediately south of Iceland, Baffin Bay, and the northern and western parts of the Nordic Seas are in all agreement with HM (Figure 4a).

Turning our attention to the surface heat fluxes, there is broad agreement between HM and ERA5 in the spatial patterns of projected and observed trends in the turbulent heat loss (Figures 4c and 4d). Specifically, the heat flux is becoming more positive (i.e., diminishing heat loss) in the subpolar gyre and the eastern portion of the Nordic Seas. In these regions, the trends in the heat flux are of the wrong sense to account for increases in STR, implying that the change in SST sensitivity is the main factor. In other specific regions, the western Greenland Seas, the eastern Baffin Bay, and the western extremity of the Labrador Sea, there is increasingly negative heat flux, which will contribute along with the previously noted increases in SST sensitivity to the increase in STR. It is noted

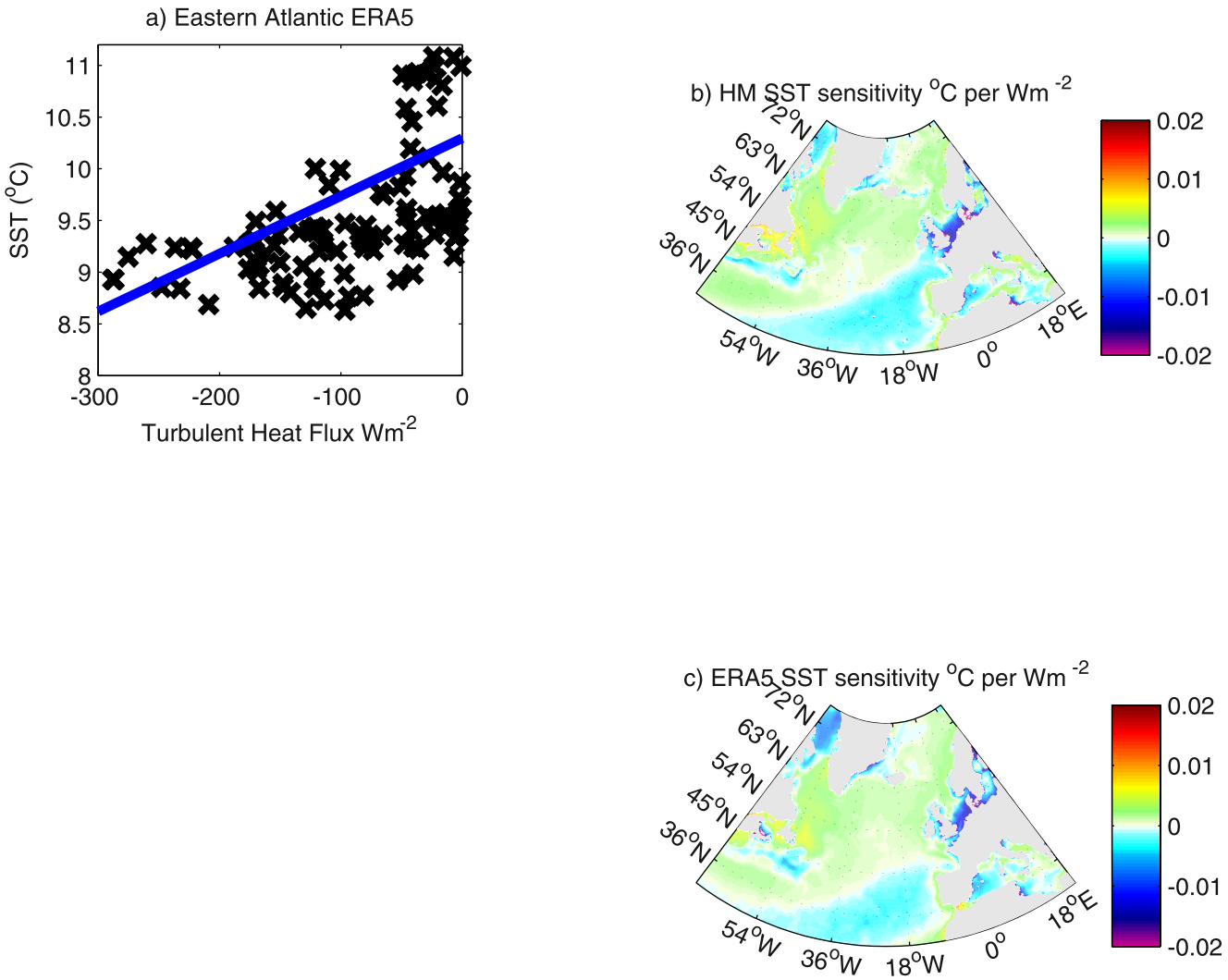

Figure 3. (a) Example plot to show the slope of daily sea surface temperature (SST) against daily turbulent heat flux (taken from ONDJF 2015–2016 ERA data). Sensitivity of SST to turbulent heat flux, as calculated from the slope of daily ONDJF SST and turbulent heat flux for (b) HM mean of 100 years 1951–2050 and (c) ERA5 mean of 40 years 1981–2020. Units are °C/Wm^{-2}.

that regions of decreased (increased) heat loss are accompanied by decreases (increases) in surface wind speed (Figures 4e and 4f), indicating the changes in surface wind are in the sense to contribute to the surface heat flux trends. It is possible that other terms for example, sea-air humidity difference and temperature difference may also play a role and we plan to explore the relative contributions in detail in subsequent work.

We have established observed and projected model based increases in STR in the mid-high latitude North Atlantic. Over much of this region, these changes are associated with corresponding changes in SST sensitivity as trends in the surface heat flux are largely of the wrong sign to cause the increase in STR. Regional exceptions to this behavior are the western Greenland Sea and eastern Baffin Bay where both the sensitivity and heat flux trends potentially contribute to the STR increase. We now turn our focus to aspects of climate change that may cause these changes in SST sensitivity, surface heat flux and subsequently STR.

3.2. Candidate Causes of Increased SST Sensitivity and Surface Heat Flux

3.2.1. Changes in Surface Stratification

It has recently been proposed that increases in late summer surface stratification lead to a stronger drop in autumn SST as the shallower mixed layer results in a smaller volume of water for surface fluxes to cool (Oltmanns

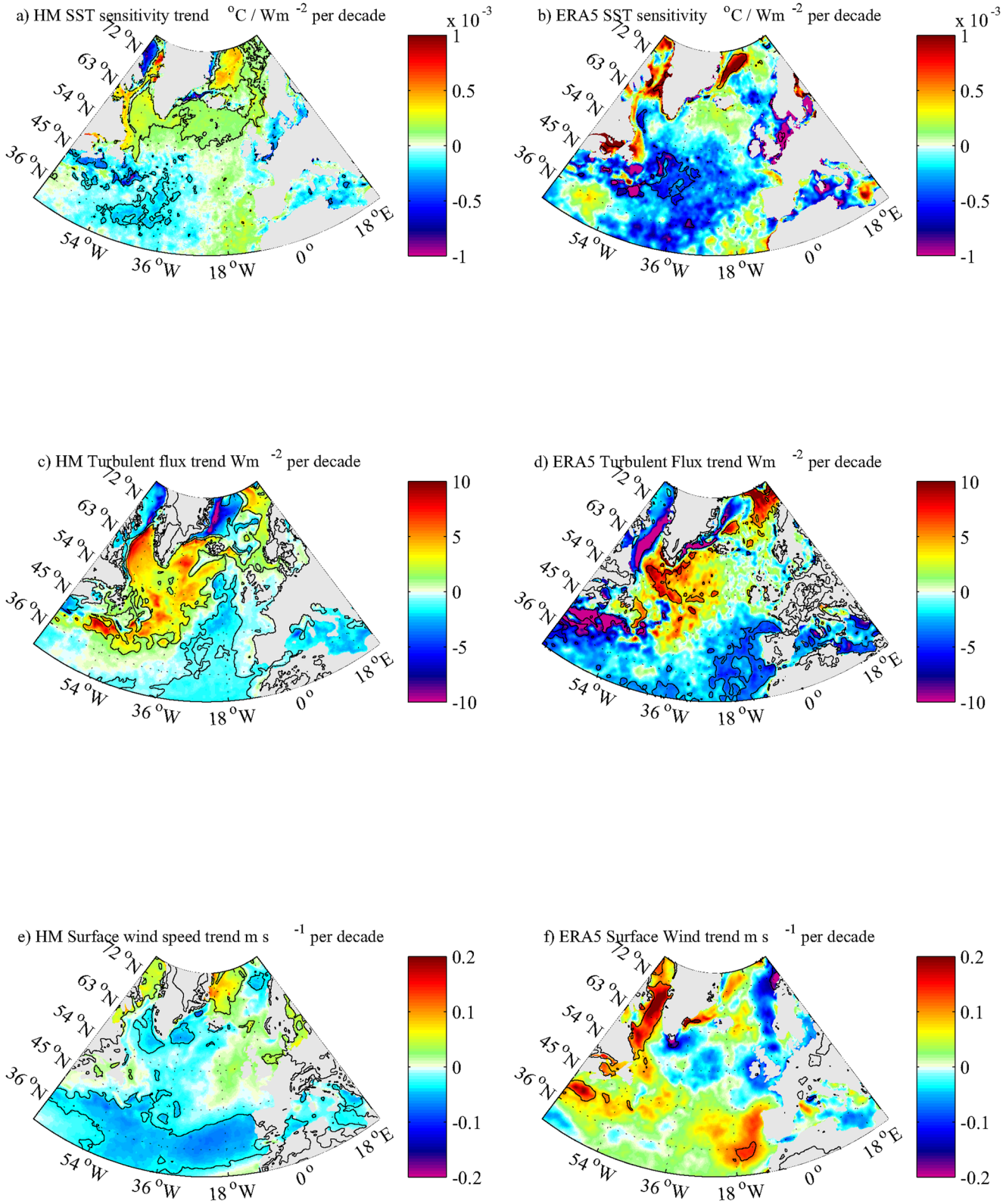

Figure 4. Trend in the ONDJF sea surface temperature sensitivity to turbulent heat flux (units °C/W m^{-2} per decade) for (a) HM 1951–2050 and (b) ERA5 1981–2020. Trend in turbulent heat flux (W m^{-2} per decade) for (a) HM 1951–2050 and (b) ERA 1981–2020. In the lower panels positive values indicate there is a reduction in ocean turbulent heat loss over time. Trend in the ONDJF surface wind speed (units m s^{-1} per decade) for (e) HM 1951–2050 and (f) ERA5 1981–2020. Black contours denote 95% significance level.

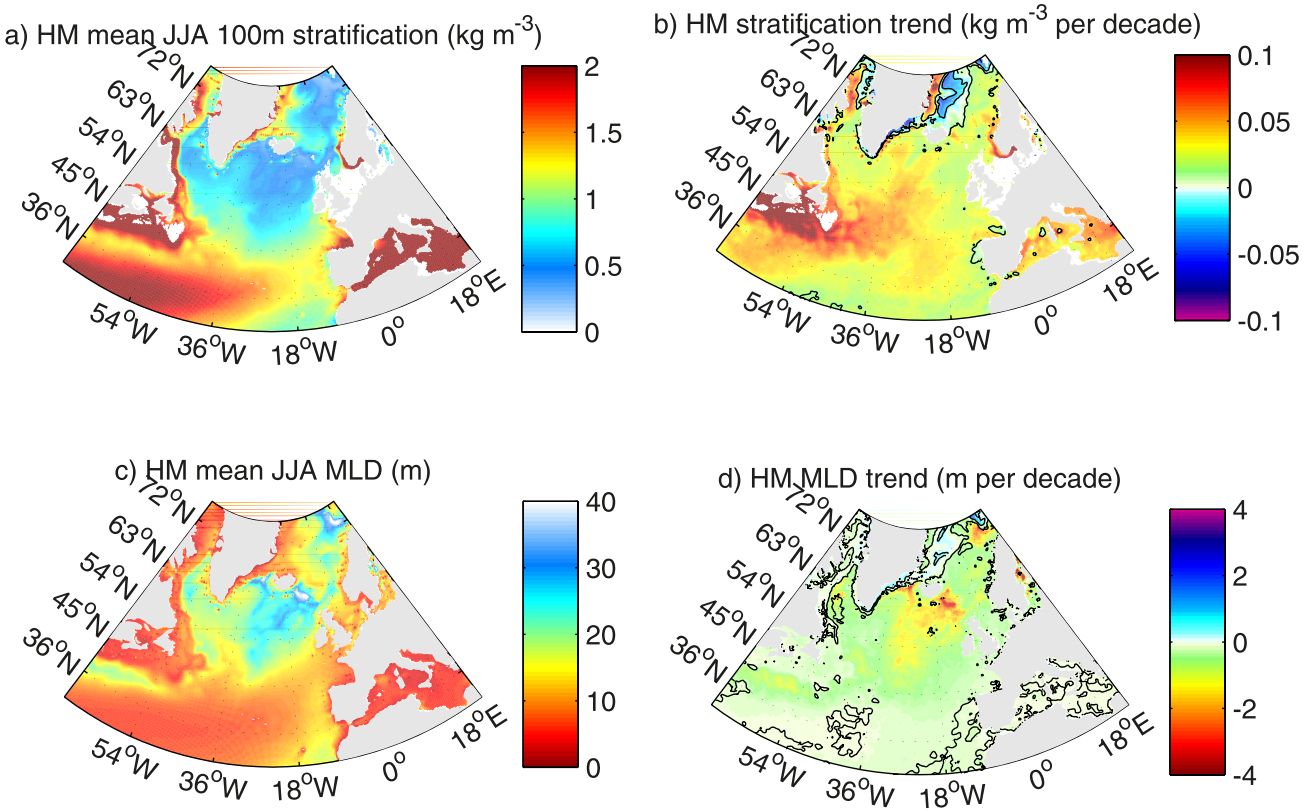

Figure 5. (a) 1951–2050 HM historical-future simulation mean JJA 100 m stratification (kg m^{-3}), (b) linear trend in 100 m stratification (kg m^{-3} per decade). (c) 1951–2050 HM historical-future simulation mean mixed layer depth (MLD, m), (b) linear trend in MLD (m per decade). Black contours denote 95% significance level.

et al., 2021). The mean and projected trend of the surface stratification are shown in Figures 5a and 5b respectively. In general, apart from the boundary current regions, the Atlantic Ocean north of 40°N is a region of relatively weak stratification. The surface stratification in the model increases in the western Atlantic, the subpolar gyre and the western Greenland Seas in the region of the West Greenland Current (the exception to this behavior is a small part of the Greenland Sea where stratification decreases). The increases in stratification are consistent with the increase in SST sensitivity particularly in the North Atlantic subpolar gyre.

For a different metric of stratification, we show the mean and trend for the summer mixed layer depth (Figures 5c and 5d), where the mixed layer depth is defined as the depth at which potential density exceeds that at the surface by more than 0.125 kg m^{-3}. Mixed Layer depth is generally small over the North Atlantic in the summer, however maximum values of about 25–30 m are found in the around 18°W and 56°N. Over most of the North Atlantic the MLD decreases, consistent with the increase in stratification. To the first order, the degree of shoaling in the mixed layer is proportional to the initial magnitude of the mixed layer. In particular, the small amount of shoaling in the subtropics reflects the very shallow (less than 10 m) mean mixed layer there. We note that the trends in neither index can completely account for the changes in sensitivity, in particularly south of 53°N and west of 20°W, where there is a negative trend in sensitivity in consistent with the trends in MLD and stratification. Although the decreases in sensitivity there are relatively weak, further work will be required to determine their causes.

3.2.2. Changes in Sea-Ice Cover

An additional process that could increase STR particularly through changes in surface heat flux is sea-ice decline. The presence of sea-ice insulates the ocean from the effects of air-sea heat exchange. Whereas sea-ice retreat will leave the ocean exposed, enabling greater surface heat loss and allowing the ocean to be more responsive to air-sea heat flux variability. Figures 6a and 6b show the decline of sea-ice in the climate change model. It can be seen that sea-ice decline is associated with an increase in SST sensitivity in the regions where stratification is less

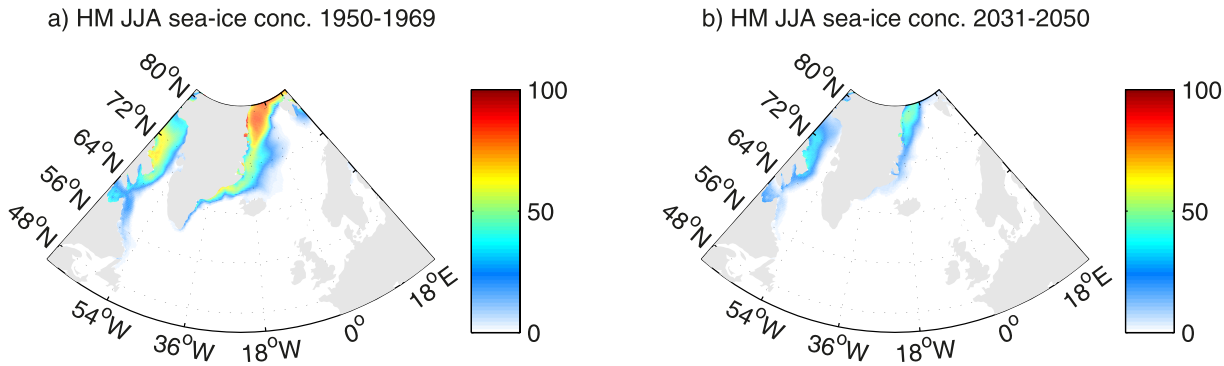

Figure 6. HM historical-future sea-ice concentration for (a) 1951–1970 and (b) 2031–2050.

important, that is the Western Nordic Seas, Denmark Strait, and the Western rim of the Labrador Sea. Similarly, there is a strong spatial correspondence between areas of sea-ice decline and regions of increased turbulent heat loss that can contribute to an increase in STR.

In general, the evidence that emerges suggests that the increases in North Atlantic STR shown in Section 3.1 are associated with increases in either or both SST sensitivity and surface fluxes depending on the area under consideration. These areas are summarized in Figure 7. Figure 7a shows the area of increasing SST sensitivity and Figure 7b shows the area of increasing heat loss. There are areas where both processes can contribute to an increase in STR, but SST sensitivity acts alone in the SPG and turbulent heat loss act alone in the western edges of Baffin and Greenland Seas. Figure 7c indicates that stratification increases in all the areas where SST sensitivity increases and Figure 7d shows that in the northern and north-western parts of the domain, the increase in turbulent heat flux corresponds strongly with areas of sea-ice decline. In summary, in areas unaffected by sea-ice changes, the increase in sensitivity is primarily associated with an increase in stratification, while in areas that undergo large decreases in sea-ice cover, a large corresponding increase in surface fluxes is important.

3.2.3. Roles of Temperature and Salinity in Increasing Stratification

Increasing surface stratification through lightening of the surface waters can occur via increasing SST or decreasing SSS. To establish the relative roles of temperature and salinity we calculate the surface stratification change that occurs when each of them is kept constant. Changes in stratification can also occur through density changes at depth (100 m), but the temporal variability there is small compared to the surface. Figure 8a shows the HM surface stratification area-averaged between 55°N and 63°N in the Atlantic basin for 1951–2050. It shows increasing surface stratification throughout the 100 years, that accelerates after 2020. Figure 8b shows the stratification change associated with changes in salinity (temperature being kept constant at the average value of the first 10 years of the time series). Similarly, Figure 8c shows the stratification change associated with changes in temperature (salinity being kept constant at the average value of the first 10 years of the time series). Comparison of Figures 8b and 8c) indicates that the projected change in SPG stratification in HM is almost entirely due to warming as opposed to freshening.

Having established the relatively minor role of long-term salinity changes in setting the mid-latitude Atlantic stratification, we now consider its influence on the interannual time scale by examining the control run. The correlation between surface stratification and both SST and SSS are shown in Figures 9a and 9b respectively. Both SSS and SST are highly correlated with the stratification, but their regions of maximum correlation are different. The regions of maximum SST correlation are south of the Denmark Strait, away from the Greenland/Labrador Boundary Current system and away from the Irminger Sea Interior. By contrast, the regions of maximum SSS correlation are north of Denmark, in the vicinity of the Greenland/Labrador Boundary Current system and in the Irminger Sea Interior. We are particularly interested if salinity sets the stratification of the subpolar gyre region as, in accordance with the mechanism proposed by Oltmanns et al. (2020), if autumn cooling in this region is enhanced it could strengthen the north-south temperature gradient, an important driver in the development of mid-latitude storms. The results of Figure 9b suggest that while SSS is an influencer of stratification as proposed by Oltmanns et al. (2020), this influence is geographically focussed, to the western rim of the North Atlantic and the Nordic Seas.

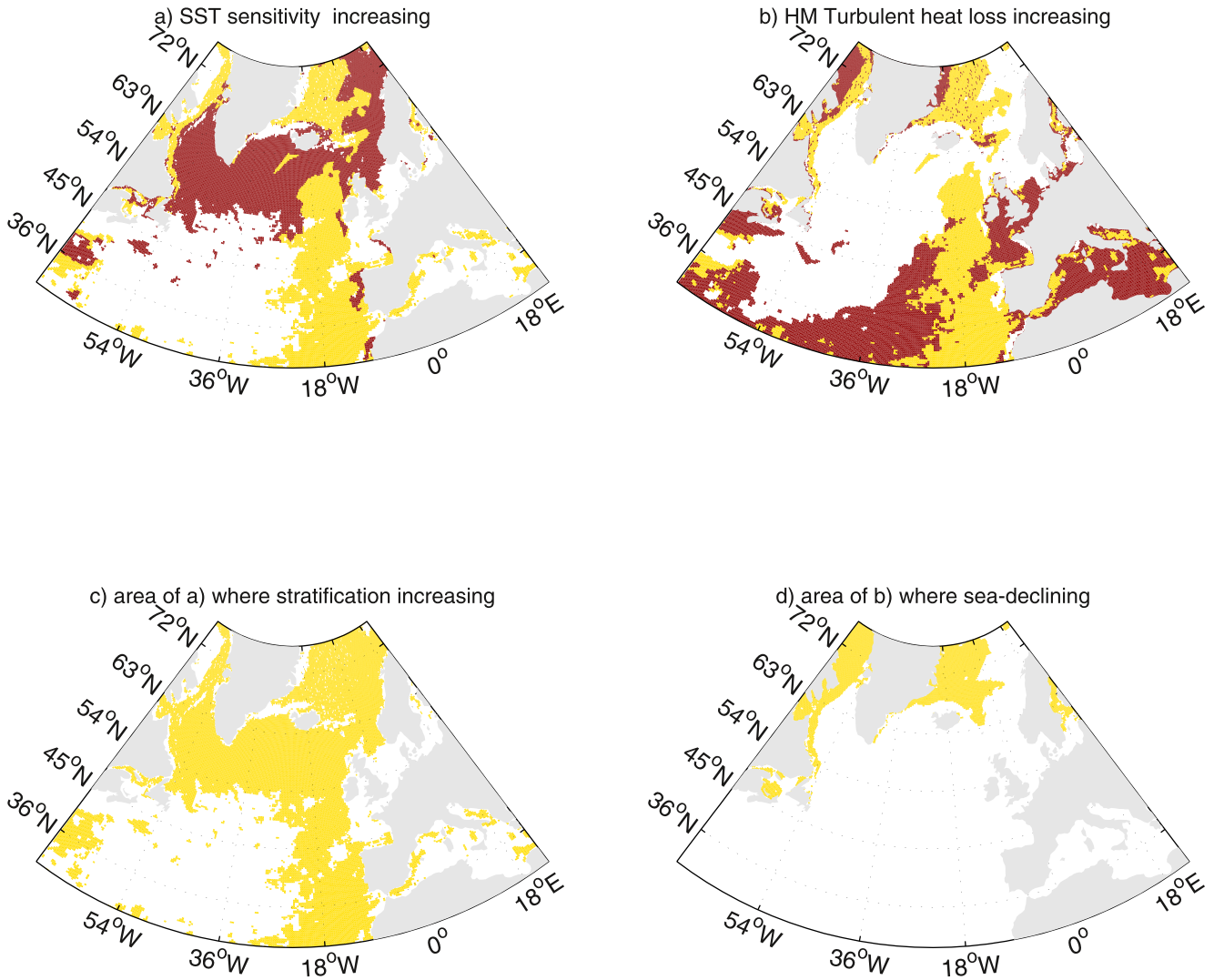

Figure 7. Shading to indicate where processes can contribute in HM to the increase in seasonal temperature reduction (STR): (a) area where sea surface temperature (SST) sensitivity increases (darker shade indicates turbulent heat loss weakening and thus does not contribute to STR increase); (c) area shaded in panel (a) where stratification increases. (b) area where turbulent heat loss increases (darker shade indicates SST sensitivity is weakening and thus does not contribute to STR increase); (d) area shaded in panel (b) where sea-ice cover decreases.

Bearing in mind that it is possible that it is only the strongest freshwater anomalies in the SPG that are able to influence summer stratification and autumn cooling, we calculate the anomalous cooling associated with 10 summers of the lowest salinity in the Labrador-Irminger Sea basin. The results (Figure 9c) indicate the extreme low salinity summers are associated with stronger than normal cooling over the whole of the subpolar gyre, the anomaly reaching up to 1°C in parts. However, upon considering the anomalous February SST following the same 10 low salinity summers, there is only a small negative SST anomaly in part of the western SPG (Figure 9d). The explanation is that the low salinity summers tend to be warmer than average. This is illustrated in Figure 9e. As a consequence, the stronger than normal cooling does not manifest itself into anomalous SST. In summary, whether one considers the long-term climate change signal or interannual variability (Oltmanns et al., 2020, 2021), the evidence from HadGEM3 does not suggest a strong influence of subpolar gyre freshwater anomalies on winter SSTs in the North Atlantic SPG.

3.3. Implications of Increased Autumn Cooling on Regional Climate

So far, we have identified a trend in increasing Autumn cooling in the mid-high latitude Atlantic Ocean. This increase in Autumn cooling is against a background of long-term warming of the Global Ocean. Here we

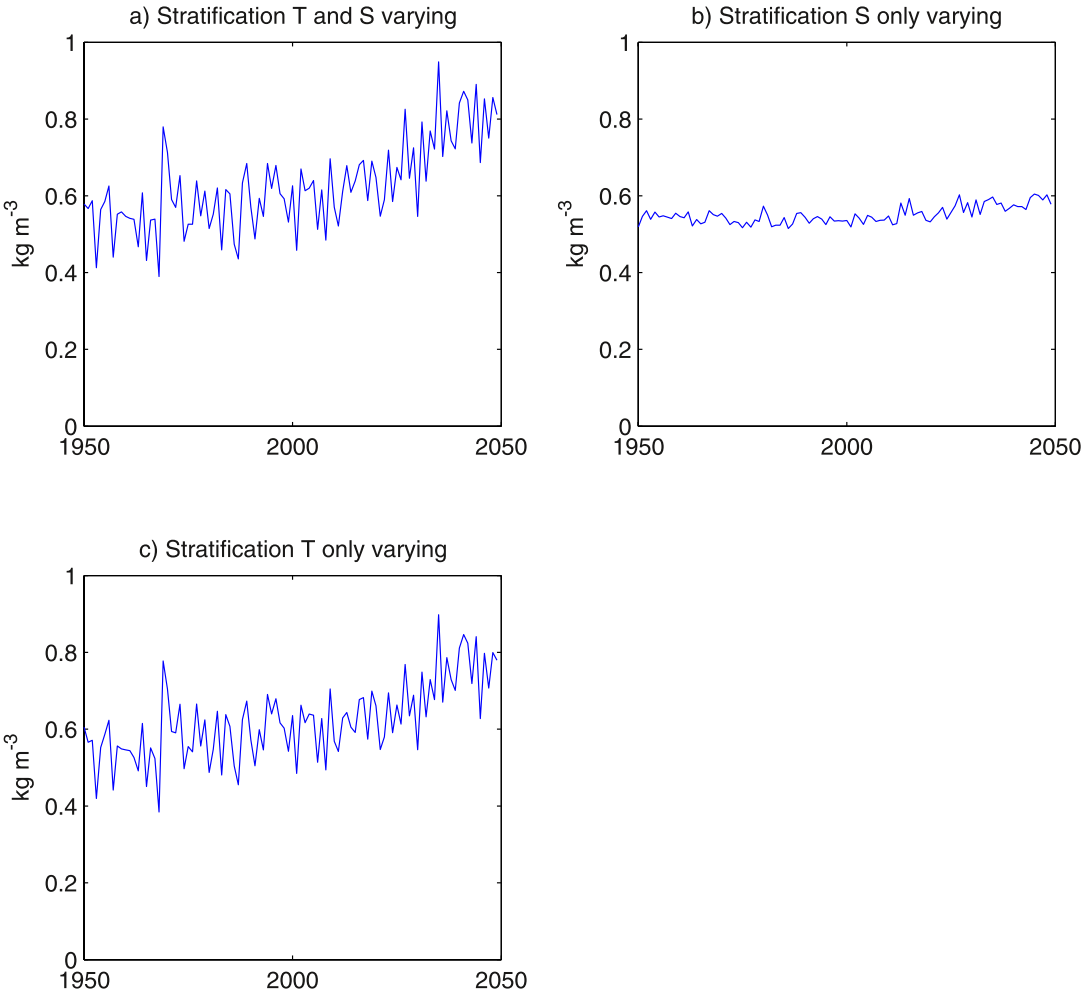

Figure 8. HM historical-future simulation area-averaged surface stratification (kg m^{-3}) for the Atlantic Basin between 55 N and 63°N (a) and (b) the same but with temperature held at constant (1951–1960) value and (c) with salinity held constant (1951–1960) value.

investigate the implications of these two changes on the large-scale meridional temperature gradient of the North Atlantic Ocean. This is of broader regional climate interest as the north-south temperature gradient is a driver of mid-latitude storm development. In Figure 10a) two regions are identified. The region to the north (SPG) is one in which the increase in Autumn cooling is more pronounced and region to the south experiences a less marked increase in Autumn cooling. If we consider the October SST, it is evident that warming occurs at approximately the same rate in STG and SPG (Figure 10b). Consequently, although there is some considerable interannual variability, there is only a modest long-term trend in the STG-SPG temperature difference (0.07°C ± 0.02°C per decade, Figure 10c). In contrast to October, in February the SPG warms at a much slower rate than in the STG (Figure 10d) and as a consequence, the STG-SPG temperature difference increases more rapidly (0.18°C ± 0.02°C per decade, Figure 10e). It should be noted that it is well documented that future changes in Atlantic SSTs and SST gradient are expected due to a combination of Global warming and changes in ocean circulation (Grist et al., 2021). In particular, a slower increase in SPG SST, known as the "warming hole" is associated with a decline in the AMOC (Drijfhout et al., 2012). However, the fact that HM shows a SPG warming rate that differs between October and February suggests that it may be necessary to appeal to changes is seasonal air-sea interaction to explain the increase in winter temperature gradient. In particular, we argue greater change in stratification/mixed layer depth in the SPG relative to the STG (Figure 5) leads to a greater change in STR in the SPG. Ultimately this results in the lower rise in February SST than in October (Figure 10d). More generally, this study suggest that SSTs become more sensitive to air-sea heat fluxes in the subpolar gyre and more exposed to turbulent heat fluxes in previously ice-covered northerly regions of the Atlantic basins.

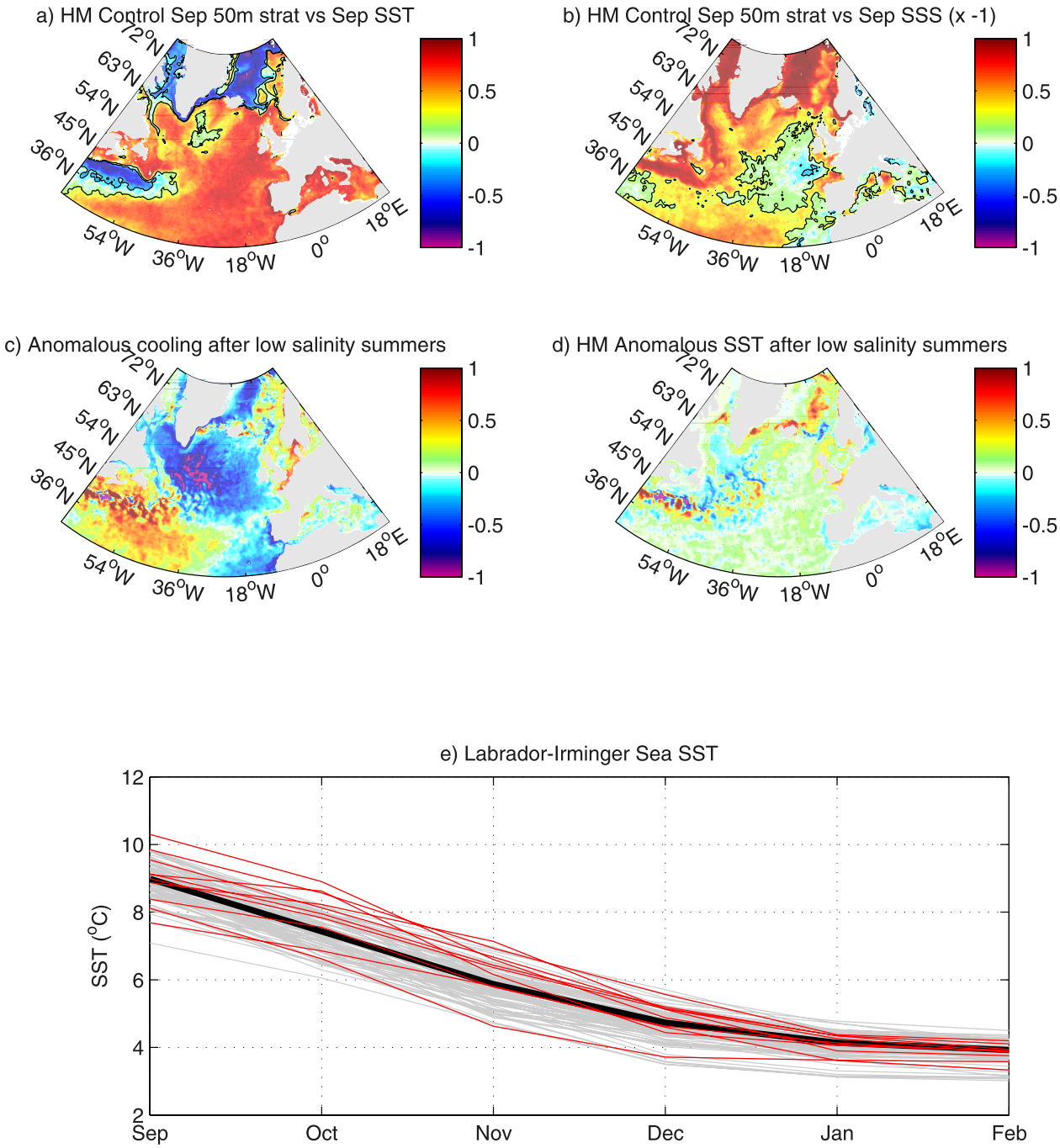

Figure 9. HM control correlation between September 50 m stratification and surface (a) sea surface temperature (SST) and (b) SSS (b) has been multiplied by −1 to allow comparison with (a). (c) Anomalous autumn SST decrease following 10 lowest salinity summers (JJA) in control run, (d) Anomalous February SST following the 10 lowest salinity summers. (e) Labrador-Irminger area SST September to February time series for 100 control years (gray lines), mean of all years (black line) and for 10 years with lowest JJA salinities (red).

4. Summary and Conclusions

We have examined changes in the Autumn SST drop, which we term the STR, in a coupled climate model and observations. Observations and climate models indicate the magnitude of the STR increases in the high-latitude Atlantic in the period 1951–2020 with trends up to 0.24°C ± 0.04°C and 0.30°C ± 0.06°C per decade respectively in the subpolar gyre. The model (observed) trends are up to 0.45 ± 0.08 (0.3 ± 0.05)

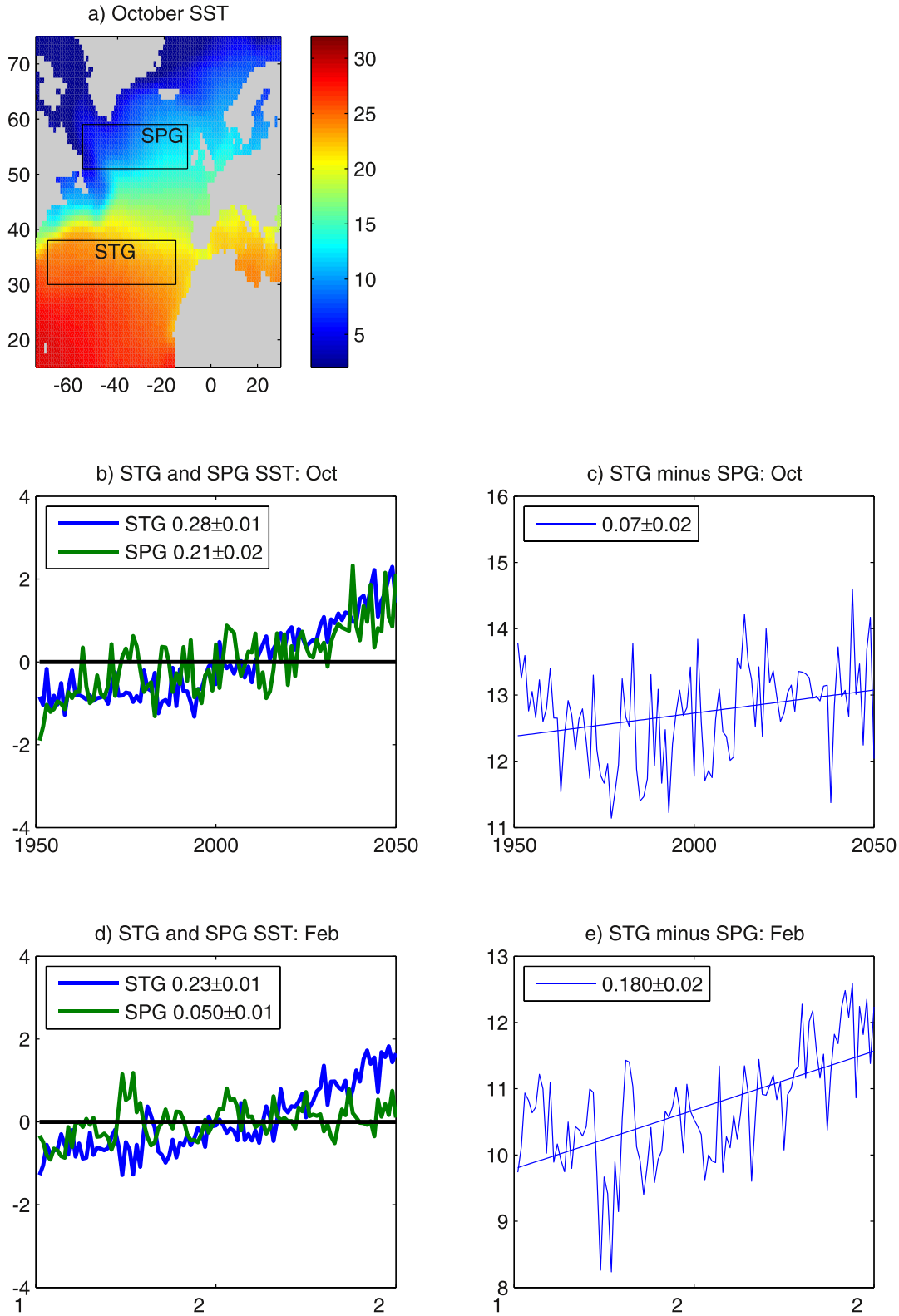

Figure 10. (a) October sea surface temperature (SST) (HadISST) and location of boxes used for area-averages. Time series of STG and SPG SST anomalies for (a) October and (b) February. Time series and linear trends of SST difference between STG and SPG for (c) October and (d) February. The trend and standard error (°C/decade) are shown in the legend. All trends are significant at 95% level.

°C per decade near the east Greenland coast. These changes have the potential to influence regional climate through their influence on the meridional SST gradient. In particular, as the increase in STR in the subpolar gyre is greater than in the subtropical gyre, the winter Atlantic meridional SST gradient increases much more than in summer. Therefore, the trends in STR have the potential to promote an increase in Atlantic winter storminess. We note here that other ocean processes, such as shifts in the Gulf Stream and a reduction in the AMOC have also been proposed as influences on North Atlantic storminess (e.g., Grist et al., 2021; Woollings et al., 2012).

Potential causes of the observed and modeled changes in STR have also been examined. In particular, changes in the two driving terms which are the autumn-winter (ONDJF) air-sea heat fluxes and the SST sensitivity to these fluxes were considered. Over most of the SPG, ONDJF turbulent heat loss from the ocean becomes weaker in recent decades, both in the model and observations. This indicates that trends in surface heat flux are not the cause of increase in STR in the SPG. The exception to this behavior are some areas where sea-ice declines and the turbulent heat loss strengthens such as the west and east Greenland coasts. In these areas, the trends in surface heat flux contribute to the trend in STR. With regard to the SST sensitivity, this has increased in most areas to the north of 54°N in the Atlantic Basin. It is thus an important reason for the increase in STR in this region, most notably in the subpolar gyre, where the other potential cause, changes in heat flux is of the wrong sign to explain the STR change.

Having established a role for SST sensitivity in STR trends in the region south of Iceland, we found that both SST sensitivity and STR were related to the surface stratification in this region. In particular, an increase in stratification, leads to an increase in the SST sensitivity to surface fluxes and in turn an increase in the STR. This is consistent with mechanisms forwarded by Chen and Wang (2015) and Alexander et al. (2018) in the context of the Tropical Pacific and zones of Large Marine Ecosystems (LMEs) respectively. Furthermore, the dominant cause of the projected increase in SPG stratification was found to be ocean warming as opposed to freshening. We note that stratification changes alone do not totally explain changes in the sensitivity of the ocean surface to heat fluxes. In principle, a change in any non-air-sea flux process that influences seasonal temperature change (e.g., mixing, entrainment, and advection) will be captured as a change in sensitivity. More generally, understanding what sets the geographical and temporal variability of SST sensitivity and how it relates to other diagnostics such as surface heat flux feedback (e.g., Frankignoul & Kestenare, 2002) is an important focus of air-sea interaction research. Further work could also utilize multiple high-resolution simulations to increase the robustness of the findings. That being the case, this study increases the body of evidence that increases in surface stratification has increased (and will continue to increase) SST sensitivity and the seasonal cycle in significant areas of the North Atlantic. Furthermore, this study highlights that surface stratification, in addition to the already often considered SST, is an important consideration for understanding the influence of the North Atlantic Ocean on regional climate.

In summary, this study has revealed through both model and observation based analyses that the seasonal autumn to winter reduction in North Atlantic SST has increased from 1950 to date and the model analysis suggests that it is projected to increase further through to 2050. This increase is predominantly associated with an increase in the sensitivity of SST change to surface turbulent heat flux. The caveat to this is that there are some regions, influenced by sea-ice decline, where ocean surface heat loss is projected to increase and in these regions this term becomes an important factor in the STR increase. Finally, the spatial variability of the increase in STR, leads to a greater winter meridional SST gradient, with potential consequences for increasing winter storminess.

Data Availability Statement

Model data used in the present analysis are available from the CMIP6 Earth System Grid Federation located via the M. Roberts (*MOHC HadGEM3-GC31-HM model output prepared for CMIP6 HighResMIP* 2018) citations in reference list. The ERA5 reanalysis data set (Hersbach et al., 2020) is available from https://www.ecmwf.int/en/forecasts/datasets/reanalysis-datasets/era5. The HadISST sea surface temperature data set (Rayner et al., 2003) is available from https://www.metoffice.gov.uk/hadobs/hadisst/.

Acknowledgments
Research was funded by the UK Research and Innovation (UKRI) projects Arcti-CONNECT (NE/V004875/1) for JG, SJ, and BS and WISHBONE (NE/T01350/1) for BS. Some of the model runs used the ARCHER UK National Supercomputing Service (http://www.archer.ac.uk).

References

Alexander, M. A., Scott, J. D., Friedland, K. D., Mills, K. E., Nye, J. A., Pershing, A. J., & Thomas, A. C. (2018). Projected sea surface temperatures over the 21st century: Changes in the mean, variability and extremes for large marine ecosystem regions of Northern Oceans. *Elementa: Science of the Anthropocene*, *6*, 9. https://doi.org/10.1525/elementa.191

Chen, C., & Wang, G. (2015). Role of the North Pacific mixed layer in the response of SST annual cycle to global warming. *Journal of Climate*, *28*(23), 9451–9458. https://doi.org/10.1175/JCLI-D-14-00349.1

Drijfhout, S., van Oldenborgh, G. J., & Cimatoribus, A. (2012). Is a decline of AMOC causing the warming hole above the North Atlantic in observed and modeled warming patterns? *Journal of Climate*, *25*(24), 8373–8379. https://doi.org/10.1175/JCLI-D-12-00490.1

Dwyer, J. G., Biasutti, M., & Sobel, A. H. (2012). Projected changes in the seasonal cycle of surface temperature. *Journal of Climate*, *25*(18), 6359–6374. https://doi.org/10.1175/JCLI-D-11-00741.1

Frankignoul, C., Czaja, A., & L'Heveder, B. (1998). Air-sea feedback in the North Atlantic and surface boundary conditions for ocean models. *Journal of Climate*, *11*(9), 2310–2324. https://doi.org/10.1175/1520-0442(1998)011<2310:asfitn>2.0.co;2

Frankignoul, C., & Kestenare, E. (2002). The surface heat flux feedback. Part I: Estimates from observations in the Atlantic and the North Pacific. *Climate Dynamics*, *19*(8), 633–647. https://doi.org/10.1007/s00382-002-0252-x

Frankignoul, C., Kestenare, E., Botzet, M., Carril, A. F., Drange, H., Pardaens, A., et al. (2004). An intercomparison between the surface heat flux feedback in five coupled models, COADS and the NCEP reanalysis. *Climate Dynamics*, *4*(22), 373–388. https://doi.org/10.1007/s00382-003-0388-3

Gallego, M. A., Timmermann, A., Friedrich, T., & Zeebe, R. E. (2018). Drivers of future seasonal cycle changes in oceanic pCO_2. *Biogeosciences*, *15*(17), 5315–5327. https://doi.org/10.5194/bg-15-5315-2018

Grist, J. P., Josey, S. A., Sinha, B., Catto, J. L., Roberts, M. J., & Coward, A. C. (2021). Future evolution of and eddy-rich ocean associated with enhanced east Atlantic storminess in a coupled model projection. *Geophysical Research Letters*, *48*(7). https://doi.org/10.1029/2021GL092719

Haarsma, R. J., Roberts, M. J., Vidale, P. L., Senior, C. A., Bellucci, A., Bao, Q., et al. (2016). High resolution model intercomparison project (HighResMIP v1.0) for CMIP6. *Geoscientific Model Development*, *9*(11), 4185–4208. https://doi.org/10.5194/gmd-9-4185-2016

Hersbach, H., Bell, B., Berrisford, P., Hirahara, S., Horányi, A., Muñoz-Sabater, J., et al. (2020). The ERA5 global reanalysis. *Quarterly Journal of the Royal Meteorological Society*, *146*(730), 1999–2049. https://doi.org/10.1002/qj.3803

Liu, F., Lu, J., Luo, Y., Huang, Y., & Song, F. (2020). On the oceanic origin for the enhanced seasonal cycle of SST in the midlatitudes under global warming. *Journal of Climate*, *33*(19), 8401–8412. https://doi.org/10.1175/JCLI-D-20-0114.1

Oltmanns, M., Holliday, N. P., Screen, J., Evans, D. G., Josey, S. A., Bacon, S., & Moat, B. I. (2021). North Atlantic freshwater events influence European weather in subsequent summers. *Weather and Climate Dynamics Discussions*. https://doi.org/10.5194/wcd-2021-79

Oltmanns, M., Karstensen, J., Moore, G. W. K., & Josey, S. A. (2020). Rapid cooling and increased storminess triggered by freshwater in the North Atlantic. *Geophysical Research Letters*, *47*(14). https://doi.org/10.1029/2020GL087207

Rayner, N. A., Parker, D. E., Horton, E. B., Folland, C. K., Alexander, L. V., Rowell, D. P., et al. (2003). Global analyses of sea surface temperature, sea ice, and night marine air temperature since the late nineteenth century. *Journal of Geophysical Research*, *108*(D14), 4407. https://doi.org/10.1029/2002JD002670

Riahi, K., van Vuuren, D. P., Kriegler, E., Edmonds, J., O'Neill, B. C., Fujimori, S., et al. (2017). The Shared Socioeconomic Pathways and their energy, land use, and greenhouse gas emissions implications: An overview. *Global Environmental Change*, *42*, 153–168. https://doi.org/10.1016/j.gloenvcha.2016.05.009

Roberts, M. (2018a). *MOHC HadGEM3-GC31-HM model output prepared for CMIP6 HighResMIP hist-1950. Version YYYYMMDD[1]*. Earth System Grid Federation. https://doi.org/10.22033/ESGF/CMIP6.6040

Roberts, M. (2018b). *MOHC HadGEM3-GC31-HM model output prepared for CMIP6 HighResMIP control-1950. Version YYYYMMDD[1]*. Earth System Grid Federation. https://doi.org/10.22033/ESGF/CMIP6.5883

Roberts, M. (2019). *MOHC HadGEM3-GC31-HM model output prepared for CMIP6 HighResMIP highres-future. Version YYYYMMDD[1]*. Earth System Grid Federation. https://doi.org/10.22033/ESGF/CMIP6.5984

Roberts, M. J., Baker, A., Blockley, E. W., Calvert, D., Coward, A., Hewitt, H. T., et al. (2019). Description of the resolution hierarchy of the global coupled HadGEM3-GC3.1 model as used in CMIP6 HighResMIP experiments. *Geoscientific Model Development*, *12*, 4999–5028. https://doi.org/10.5194/gmd-12-4999-2019

Saba, V. S., Griffies, S. M., Anderson, W. G., Winton, M., Alexander, M. A., Delworth, T. L., et al. (2016). Enhanced warming of the Northwest Atlantic Ocean under climate change. *Journal of Geophysical Research: Oceans*, *121*(1), 118–132. https://doi.org/10.1002/2015JC011346

Santer, B. D., Wigley, T. M. L., Boyle, J. S., Gaffen, D. J., Hnilo, J. J., Nychka, D., et al. (2000). Statistical significance of trends and trend differences in layer-average atmospheric temperature time series. *Journal of Geophysical Research*, *105*(D6), 7337–7356. https://doi.org/10.1029/1999/JD901105

Sobel, A. H., & Camargo, S. J. (2011). Projected future seasonal changes in tropical summer climate. *Journal of Climate*, *24*(2), 473–487. https://doi.org/10.1175/2010JCLI3748.1

Timmermann, A. F., Jin, F., & Collins, M. (2004). Intensification of the annual cycle in the tropical Pacific due to Global Warming. *Geophysical Research Letters*, *31*(12), L12208. https://doi.org/10.1029/2004GL019442

Williams, K. D., Copsey, D., Blockley, E. W., Bodas-Salcedo, A., Calvert, D., Comer, R., et al. (2017). The met office global coupled model 3.0 and 3.1 (GC3.0 and GC3.1) configurations. *Journal of Advances in Modeling Earth Systems*, *10*(2), 357–380. https://doi.org/10.1002/2017MS001115

Woollings, T., Gregory, J. M., Pinto, J. G., Reyers, M., & Brayshaw, D. J. (2012). Response of the North Atlantic storm track to climate change shaped by ocean–atmosphere coupling. *Nature Geoscience*, *5*, 313–317. https://doi.org/10.1038/ngeo1438